Chinese Journal of
POLYMER SCIENCE

RESEARCH ARTICLE

https://doi.org/10.1007/s10118-026-3612-y
Chinese J. Polym. Sci.

Ceramizable Perforated Silicone Foam for Thermal Insulation and Refractory Building Materials

Xiang-Yuan Tian, Xin Zhang, Dian-Bo Zhang, Ya Liu, Xiao-Pei Wang*, and Zhen-Xiu Zhang*

Key Laboratory of Rubber-Plastics, Ministry of Education/Shandong Provincial Key Laboratory of Rubber-Plastics, Qingdao University of Science and Technology, Qingdao 266042, China

Electronic Supplementary Information

Abstract Liquid silicone rubber foam (LSRF) offers superior processability, high mechanical flexibility, and low thermal conductivity, which are of great significance for achieving long-term thermal insulation and fire resistance but remain challenging to achieve. We first prepared LSRF with excellent open-cell performance, achieving a water absorption rate of 242.5%, and then explored the advantages of flame-retardant solution impregnation in the open-cell structure. Meanwhile, the synergistic flame-retardant effect of kaolin (KL), glass powder (GP), and silica aerogel (AG) was investigated. When the composite formulation was LSRF/30KL10GP20AG, the material exhibited outstanding flame-retardant properties: the limiting oxygen index (LOI) reached 33.2%, an increase of 9% compared with unfilled LSRF, the vertical burning rating was V-0, and the water contact angle of the surface after combustion was 160.35°, meeting the superhydrophobic standard. At the same time, the sample LSRF/30KL10GP20AG showed a 49.6% reduction in peak heat release rate and an 83.8% reduction in total peak smoke production compared to LSRF. Under butane-flame impingement at 1300 °C, the flame-retardant LSRF maintained an intact structure for 120 s, with the backside temperature rising only to 219 °C, demonstrating excellent thermal insulation performance. In a high-temperature environment at 800 °C, the foam well retained its original cell structure and maintained volume stability, forming a dense, hard ceramicized carbon layer with a compressive strength of 2.69 MPa. The fillers were uniformly impregnated and distributed on the foam surface and cell walls, endowing the material with durable flame retardancy, low smoke generation, and minimal toxic gas release, effectively inhibiting the spread of flames during fires and enabling LSRF foam to be widely applied in the field of building flame retardancy.

Keywords Liquid silicone rubber foam; Vacuum impregnation; Flame-retardant; Thermal insulation; Ceramization

Citation: Tian, X. Y.; Zhang, X.; Zhang, D. B.; Liu, Y.; Wang, X. P.; Zhang, Z. X. Ceramizable perforated silicone foam for thermal insulation and refractory building materials. *Chinese J. Polym. Sci.* https://doi.org/10.1007/s10118-026-3612-y

INTRODUCTION

Liquid silicone rubber foam (LSRF) possesses inherent properties, including excellent chemical solvent resistance, UV resistance, ozone resistance, and electrical insulation, making it widely used in aerospace, construction, and other fields.[1] Due to its low density and thermal conductivity, LSRF is widely used as a thermal insulation material for buildings.[2] However, the flammability of LSRF poses a serious threat to buildings and personnel, limiting its promotion in fire prevention applications. Adding flame retardants is a conventional strategy to enhance the flame retardancy of foams, but most flame retardants require high doses to be effective when used alone.[3,4] Moreover, even if LSRF achieves flame retardancy, its mechanical properties and lightness will be affected. Additionally, it tends to thermally decompose into a loose structure at high temperatures, leading to severe structural damage.[5] Consequently, the fabrication of ultra-high temperature-resistant LSRF with excellent thermal insulation, flame retardancy, and fire resistance is of great significance.

With advances in composite materials technology, incorporating ceramifiable components into polymer matrices has emerged as an effective strategy to enhance the fire resistance and protective performance of materials. Based on this concept, ceramifiable silicone rubber composites have been developed, composed primarily of three components: a silicone rubber matrix, a fluxing agent, and a refractory filler.[6] When exposed to open flame, the fluxing agent first melts to form a liquid phase, which then infiltrates the refractory filler and undergoes a eutectic reaction with SiO_2 generated by the pyrolysis of silicone rubber, ultimately forming a ceramic protective layer with a continuous structure and high strength that effectively blocks heat flux and flame spread.[7] Shang *et al.*[8] prepared ceramifiable flame-retardant room-temperature vulcanized silicone rubber foam using glass powder and mica powder as fluxing agents, respectively, and aluminum hydroxide as the refractory filler. Their studies demonstrated

* Corresponding authors, E-mail: xiaopeiwang@qust.edu.cn (X.P.W.)
E-mail: zhangzhenxiu@qust.edu.cn (Z.X.Z.)

Received November 24, 2025; Accepted February 4, 2026; Published online April 9, 2026

that mica powder and aluminum hydroxide exhibit a more efficient synergistic flame-retardant effect along with favorable ceramifiability. Lin *et al*.[9] introduced a silane coupling agent into expandable graphite as a flame retardant, and further added montmorillonite and zinc borate as the refractory filler and fluxing agent. This approach endowed the foam with a denser microstructure, improved its mechanical strength and flexibility, and enhanced its ceramification performance. However, the resulting ceramic protective layer was weak and lacked thermal insulation, rendering it ineffective at protecting the internal structure during combustion. Meanwhile, achieving complete ceramification requires a high filler content, which not only leads to poor filler dispersion in the foam and interferes with the foaming process but also significantly degrades properties such as the material's apparent density. More critically, even with such high filler loading, the material still struggles to protect the internal structure from flame erosion.[10]

Compared with direct mixing, the open-cell impregnation filling method enables the impregnation of ceramifiable flame-retardant fillers into open-cell foam materials, allowing the flame-retardant effect to penetrate both the surface and interior of the material. During combustion, the flame first attacks the flame-retardant fillers rather than the matrix, endowing the foam with the functions of both a flame-retardant coating and blended flame retardants without interfering with the foaming process. Han *et al*.[11] surface-treated supercritical silicone rubber foam with a ceramifiable talc/APP/CB coating, which not only gave full play to the synergistic effect between the fillers and effectively reduced the flammability of the silicone rubber foam but also enhanced the strength of the silicone rubber foam after combustion. Wang *et al*.[12] treated open-cell PU foam with a flame-retardant coating composed of multiple fillers, resulting in a synergistic flame-retardant effect among the various components in the coating, significantly reducing the flammability of the coated PU foam without affecting its porous structure and mechanical properties. Meanwhile, in the research field of ceramifiable silicone rubber, the application exploration of flame-retardant fillers KL and GP has undergone years of development. However, to date, they have not achieved the ideal effect, meeting practical application expectations for material ceramification efficiency, high temperature structural stability, and synergistic optimization of comprehensive properties.[13] Therefore, we propose that on the basis of KL and GP, introducing SiO_2 aerogel can not only enhance the ceramified protective layer but also improve the thermal insulation performance of the material. This enables effective resistance to heat conduction inward during combustion, thereby maintaining the cell structure and ensuring long-term effective flame retardancy.

To address the aforementioned challenges, this study selected four pore-opening agents with different particle sizes: NaCl, sucrose A/B, and poly(ethylene oxide) (PEO). First, the AB-component liquid silicone rubber was subjected to a pore-opening treatment to systematically control the foam's porosity, open-cell rate, and density. Subsequently, through the vacuum impregnation-high temperature drying process, ceramifiable flame-retardant fillers (KL, GP, AG) with high synergistic effects were introduced into both the surface and the interior of the Perforated foam. The core mechanism lies in the connection and mutual enhancement of three effects: promoting char formation, melting sealing, and nano-thermal insulation. This enables the foam to form a high-strength char-layer framework during high-temperature combustion, resulting in a tough, dense, highly thermal-insulating, and multifunctional protective layer. The research aims to develop silicone rubber foam materials that integrate lightweight, flame-retardant, and high-strength ceramification properties, providing a new technical path to address the multifunctional integration problem in high-end fields.

EXPERIMENTAL

Material

AB two-component foaming silicone, purchased from Huizhou Fulda Technology Co., Ltd. Sodium dodecyl sulfate, table salt (NaCl), poly(ethylene oxide) (PEO) (molecular weight: 1000), sucrose A (particle size: 500 μm), sucrose B (particle size: 100 μm), calcined kaolin (KL), and glass powder (GP) were all commercially available. Silica aerogel (particle size of 0–1 mm), purchased from IBI and New Materials Co., Ltd. Liquid silicone rubber (Dow Corning 184) (viscosity: 5100 cP), purchased from Dow Chemical Co., Ltd.

Preparation

Preparation of perforated foam

Different mass fractions of pore-forming agents (NaCl, sucrose A, sucrose B, PEO) were added to the AB two-component foaming silicone, followed by 0.4 phr of sodium dodecyl sulfate. The mixture was mechanically stirred for 10 min, poured into a mold for pre-curing for 2 min, and then shaped. It was then placed in a 60 °C oven for chemical foaming for 10 min to obtain silicone rubber foam. The resulting silicone rubber foam was soaked in deionized water for 2 h, then subjected to ultrasonication for 2 h to remove the pore-forming agents, ultimately obtaining porous liquid silicone rubber foam material. The preparation precess is shown in Fig. 1.

Preparation of ceramicizable composite silicone foam

Different mass fractions (20 parts of AG recorded as 20AG) of KL, GP, AG, and Dow Corning 184 silicone were weighed into a beaker, and a specified amount of *n*-hexane was added to dissolve them. Mechanically stirred for 2 h, followed by ultrasonic dispersion for 1 h, and then mechanically stirred for another 2 h to mix evenly, obtaining a ceramic flame-retardant solution. The prepared open-cell silicone foam was added into the ceramic flame-retardant solution and vacuum-impregnated for 30 min, repeated for 3 times. After impregnation, the samples were weighed and placed in an oven to dry for 24 h. After drying, the samples were removed, and depending on the amount of flame-retardant filler added, the resulting samples were named as LSRF, LSRF/20AG, LSRF/30KL10GP, LSRF/10KL30GP20AG, LSRF/20KL20GP20AG, and LSRF/30KL10GP20AG, respectively. The detailed formulation list is shown in Table S1 (in the electronic supplementary information, ESI). The preparation precess is shown in Fig. 2.

Characterization and Measurements

Microstructure analysis

The silicone rubber foam samples were cooled in liquid nitrogen and then fractured. The fractured surfaces were facing up-

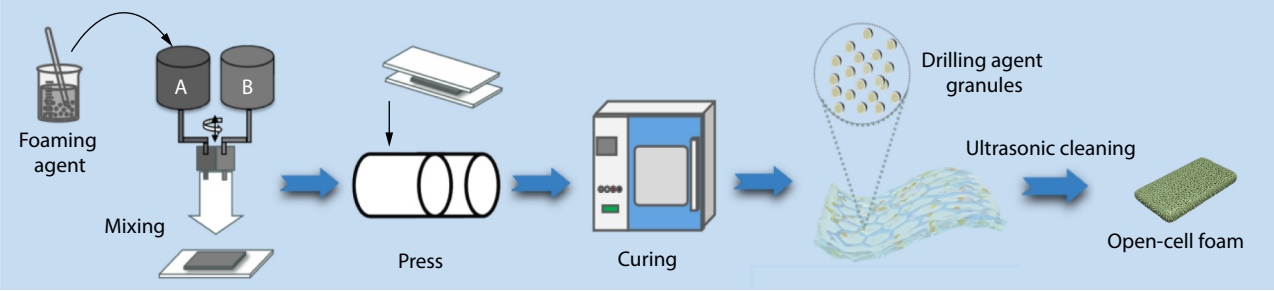

Fig. 1 Perforated foam preparation process diagram.

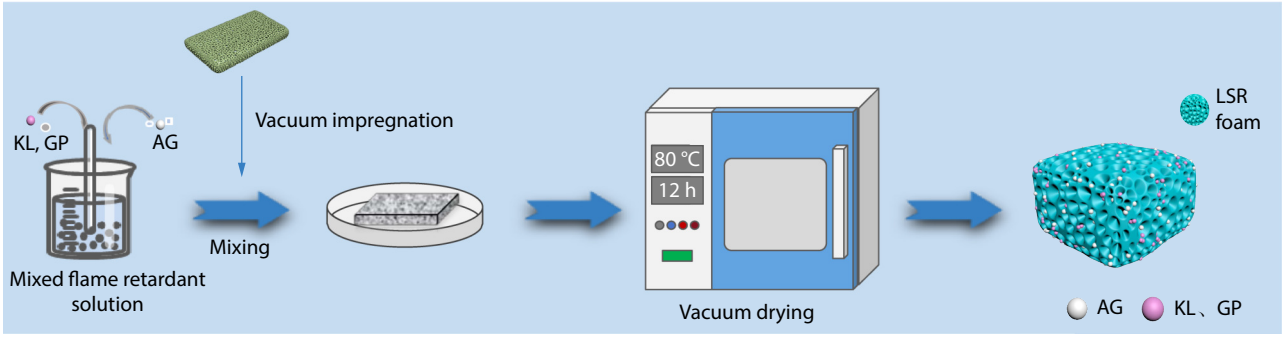

Fig. 2 Preparation process diagram of ceramicable open-cell flame-retardant silicone foam.

wards and attached to the specimen stage using conductive adhesive. After gold sputtering treatment on the fracture surface, the cross-sectional structure of the samples was observed using a scanning electron microscope (SEM).

Water absorption, porosity, and apparent density tests

The water absorption rate of the samples was determined in accordance with ASTM D570-98. The samples were completely immersed in distilled water at room temperature (25 °C). The weight of each sample was then monitored at 30-min intervals until the total immersion duration reached 300 min. The initial weight of the samples at the start of immersion was recorded as m_1, and the weight after the completion of immersion was recorded as m_2. Subsequently, the density of the samples after immersion ρ_1 was measured using a densitometer. The apparent density (ρ), water absorption rate (W_1) and porosity rate (W_2) were then calculated using Eqs. (1), (2) and (3), respectively.

$$\rho = \frac{m_1}{m_2} \times \rho_1 \quad (1)$$

where m_1 is the mass before soaking, m_2 is the mass after soaking, and ρ_1 is the density after soaking.

$$W_1 = \frac{m_2 - m_1}{m_1} \times 100\% \quad (2)$$

where m_1 is the mass before soaking, and m_2 is the mass after soaking.

$$W_2 = \frac{\rho - \rho_0}{\rho_0} \times 100\% \quad (3)$$

where ρ_0 is the density of the dense liquid silicone rubber, and ρ is the apparent density.

Mechanical performance testing

The samples are cut into rectangular foam pieces measuring 20 mm × 20 mm × 5 mm. Using an electronic universal testing machine, they are compressed at 60 mm/min for 10 cycles, with deformation and stress recorded during the test.

Thermal analysis

Thermal analysis tests of the samples were conducted using a Mettler TG50 thermogravimetric analyzer and a TG-IR tester, including thermogravimetric analysis and testing of gases generated during the thermal decomposition of silicone flame-retardant foam. The samples to be tested were heated at 10 °C/min from 30 °C to 900 °C under a nitrogen flow of 10 mL/min.

Thermal conductivity test

The thermal conductivity of the samples was measured using a DTC-300 thermal conductivity meter. The samples were fabricated into circular discs with a diameter of (50±0.25) mm and a thickness of (5.0±0.5) mm, and the tests were conducted at 30 °C.

Contact angle test

The apparent contact angle (APCA) and contact angle hysteresis (CAH) of 4 μL of water droplets on the sample surface were measured using a contact angle analyzer (Kruss DSA100, Germany). The average value of three measurements was determined. To ensure that 4 μL of water droplets were successfully deposited on the surface, an ultra-fine syringe needle with an inner diameter of only 0.03 mm, which was also hydrophobically treated with FAS-17, was selected. A high-speed camera (Photron Mini 100 and Olympus i-speed 716) was used to record droplet impact on the sample surface at 1×10^4 frames per second, and contact time was directly measured from the CCD camera.

Flame impact test

The flame impact test was conducted using a flame impact evaluation device, and the actual temperature changes on the back surface of the sample were recorded with an infrared thermal imager. The sample dimensions were 100 mm × 100 mm × 10 mm. Meanwhile, at room temperature, the thermal conductivity of the silicone flame-retardant foam was measured using a

Hot Disk thermal constants analyzer, with sample dimensions of 10 mm × 10 mm × 2 mm.

Limiting oxygen index (LOI) test

The burning performance of silicone flame-retardant foam was tested using an HC-2 oxygen index tester in accordance with GB/T 2406.2-2009. The sample size was 100 mm × 10 mm × 10 mm. A digital camera and a desktop scanning electron microscope were used to photograph and record the testing process and the sample morphology for subsequent analysis.

Vertical burning test

Using the CZF-3 horizontal-vertical burning tester, the vertical burning (UL-94) classification of silicone rubber foam was evaluated according to GB/T 2408-2021. The dimensions of all specimens were 120 mm × 13 mm × 12 mm.

Cone calorimeter test

The cone calorimeter test (CCT) was conducted in accordance with the ISO 5660-1993 standard at a heat flux of 25 kW/m^2. The samples were cut into dimensions of 100 mm (length) × 100 mm (width) × 4 mm (thickness). For the test, the samples were wrapped in aluminum foil and placed horizontally on the test platform. Digital camera was used to capture the photographs of char residues after the test.

Ceramization performance test

The foam samples (50 mm × 50 mm × 5 mm) are placed in a muffle furnace and heat-treated at 800 °C for 1 h each. After cooling to room temperature, the ceramic block samples are taken out, and their 50% compressive stress is measured using an electronic universal testing machine manufactured by Greatwell Scientific Instruments Co., Ltd. according to GB/T 8489-2006, in order to assess the ceramization performance of LSRF.

RESULTS AND DISCUSSION

Pore Structure of LSRF

Fig. 3 and Fig. S1 (in ESI) show the micromorphological structures of foams prepared with different pore-opening agents. Fig. 3 illustrates that the foam prepared with NaCl as the pore-opening agent has a relatively large cell size (average 712 μm at 125 phr). This phenomenon is attributed to the fact that NaCl has little effect on cells and does not inhibit foaming.[14] Compared with sucrose A, sucrose B, due to its smaller particle size (Fig. S2 in ESI), disperses more uniformly in the silicone rubber. With increasing dosage, cell size reaches its smallest and most uniform (average 448 μm at 125 phr), and the pore-opening effect is also better. Although PEO has a small particle size, it exhibits viscous flow in solution, leading to residues during pore opening. This further results in uneven pore formation and a high residual amount in the foam, ultimately weakening the pore-opening effect of material, with an average cell size of only 488 μm at 125 phr. Studies indicated that the employment of 125 phr sucrose B as the pore-opening agent yields a foam with not only a more uniform cellular structure but also a better pore-opening performance. The homogeneous distribution of cells improves the overall material properties, while the favorable pore-opening effect further enhances pore connectivity and functionality in the foam.

Porosity, Water Absorption, and Density of LSRF

Fig. 4 further elucidates that the influence of different types and dosages of pore-opening agents on the porosity (Fig. 4a) and water absorption (Fig. 4b) of the foam. The type, content, and pore-forming mechanism of the pore-opening agent exert a synergistic regulatory effect on the porosity and water absorption of the foam. The porosity and water absorption of the four pore-opening agents both exhibit a continuous upward trend with increasing content. This phenomenon indicates that the pore-opening agent effectively improves the connectivity of the foam's pore structure and the proportion of pore space through the pore-forming and pore-opening mechanism, and the higher the content, the greater the porosity improvement. Further comparison among different pore-opening agents reveals that, benefiting from its smaller particle size, larger specific surface area, and more homogeneous dispersion, sucrose B can form finer pores with superior channel connectivity at the same dosage. Consequently, both the growth rate and peak value of porosity and water absorption for sucrose B are significantly higher than those of other pore-opening agents, which fully reflects the key role of particle size in regulating the pore-opening effect.[15] However, it is noteworthy that the superiority of the pore-opening effect is not entirely determined by particle size. Despite its small particle size, PEO exhibits much lower porosity and water absorption than sucrose B, which is closely associated with the intrinsic chemical properties of PEO.[16] Collectively, the above results demonstrate that the foam material prepared with 125 phr sucrose B as the pore-opening agent achieves optimal performance in both water absorption and porosity, providing important insights for the optimal design of foam materials.

The regulatory effect of four pore-opening agents on foam density is depicted in Fig. 5. As the addition amount of pore-opening agents increases from 0 phr to 125 phr, the foam density of all systems exhibits a decreasing trend (Fig. 5a), confirming that pore-opening agents achieve material lightweight by constructing interconnected pore structures.[17] Among them, the density of the NaCl system decreases from 0.323 g/cm^3 to 0.270 g/cm^3, and its dissolution-type pore-forming mechanism is effective but limited by pore channel uniformity. The density of the sucrose A system decreases gently to 0.268 g/cm^3, while the sucrose B system shows the largest density reduction, dropping to 0.259 g/cm^3 at 125 phr. Its small particle size and good dispersibility enable the formation of uniform and dense pore channels in the foam, reflecting the synergistic regulation of particle dispersibility and pore-forming effect. It ultimately reaches the lowest density of 0.259 g/cm^3 at 125 phr, a phenomenon attributed to the competitive mechanism between the filling effect at low addition amounts and the pore-forming effect at high addition amounts.[18] The PEO system has a relatively limited lightweight effect due to its high viscosity after dissolution, which makes it difficult to precipitate. Notably, Fig. 5(b) intuitively demonstrates the excellent lightness of the Perforated foam prepared with the sucrose B system, and its ability to stably place on thin branches verifies the material's outstanding lightweight performance. In conclusion, the above results indicate that sucrose B exhibits the optimal density regulation effect of 0.259 g/cm^3 at 125 phr.

https://doi.org/10.1007/s10118-026-3612-y

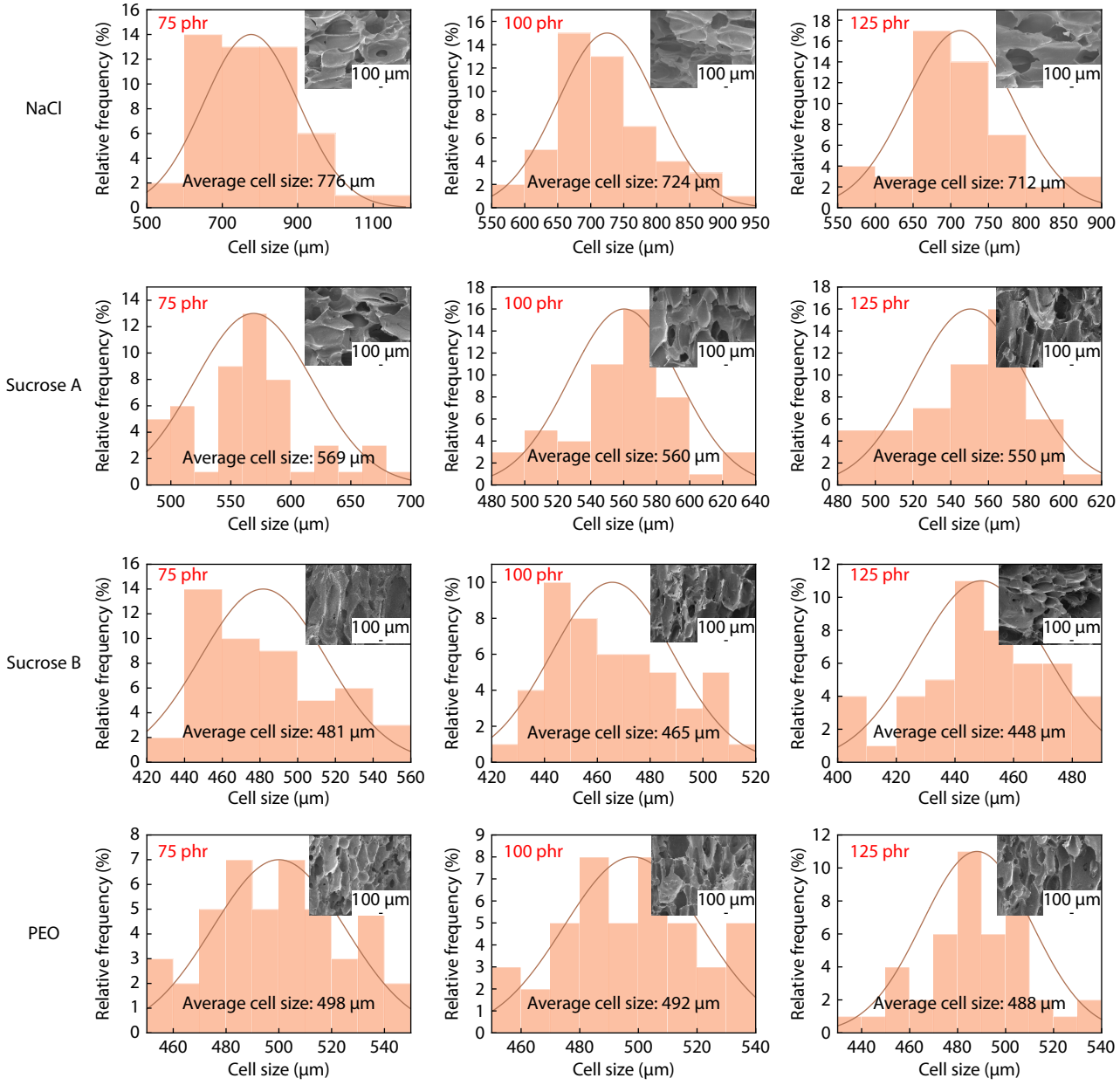

Fig. 3 Effect of different amounts of pore-opening agent on pore structure and size.

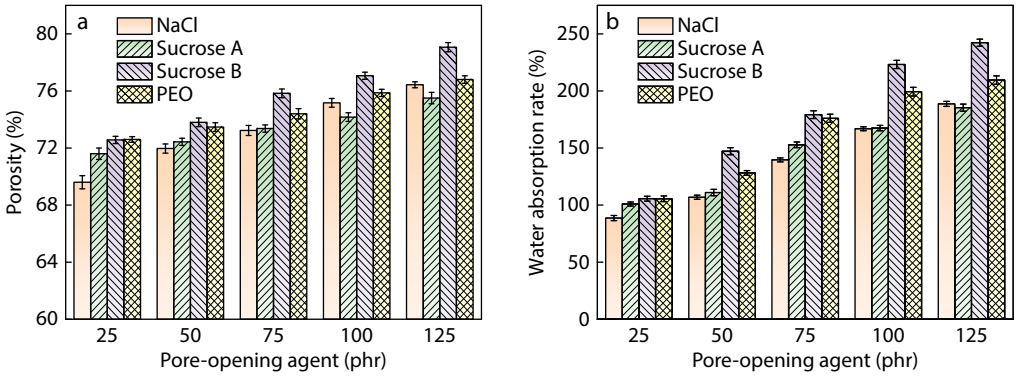

Fig. 4 The effects of different types and amounts of pore-opening agent on the (a) porosity and (b) water absorption of the foam.

https://doi.org/10.1007/s10118-026-3612-y

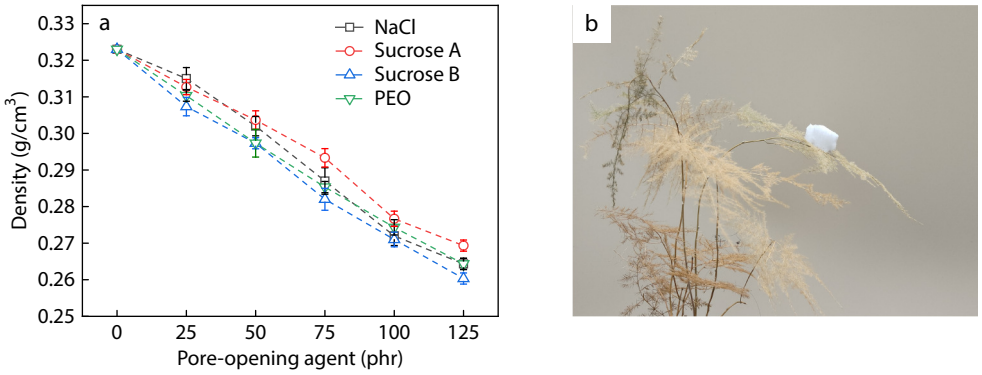

Fig. 5 (a) Effect of different types and amounts of pore-opening agent on foam density; (b) Lightweight display.

Compressive Properties of LRSF Composites

Fig. 6 effectively displays the influence of different filler systems on the cyclic compressive properties and compressive strength of foam materials. As observed in Fig. 6(a), the compressive stress increases continuously with strain, with a pronounced rate of increase at high strains (>60%), reflecting the typical mechanical response of pore compression, matrix densification, and filler stress transfer.[19] A comparison of compressive properties across filler systems shows that the unfilled LSRF sample relies solely on matrix elastic deformation, resulting in the lowest compressive stress. The sample with only 20AG filler shows improved performance due to rigid particle reinforcement, but the enhancement effect remains limited. As filler content increases, the LSRF/30KL10GP sample exhibits superior stress growth characteristics. The further-optimized samples (LSRF/10KL30GP20AG, LSRF/20KL20GP20AG, and LSRF/30KL10GP20AG) have constructed dense reinforcing networks through multiscale particle filling and interfacial interactions.[20] Fig. 6(b) presents the compressive strength of different flame-retardant LSRF samples. With formulation optimization, the compressive strength shows an upward trend. Among them, the LSRF/30KL10GP20AG sample shows the most pronounced response, with a peak stress of 986 kPa. Collectively, these results confirm that filler synergism plays a decisive role in improving the compressive properties of foam materials, and optimizing filler combinations can significantly enhance the materials mechanical performance.

Thermal Stability of LRSF Composites

The differences in thermal properties of foams with different fillers are exhibited in Fig. 7. The mass of all samples begins to decrease slowly at 200 ℃ is disclosed in Fig. 7(a). The reason for this is that the organic matrix components in the material (such as weak bonds on silicone rubber molecular chains and additives) initiate thermal decomposition at this temperature, releasing small-molecule volatiles and thus causing mass loss. In the temperature range of 400–600 ℃, the mass loss rate accelerates significantly, which is the intense stage of thermal decomposition. Combined with the sharp mass loss peak in the DTG curve (Fig. 7b), which can be explained by the main chain structure of silicone rubber undergoes large-scale cracking in this temperature range. Simultaneously, the synergistic effect between the fillers and matrix is activated, with partial fillers participating in the ceramification reaction to suppress excessive matrix degradation. Individually, the LSRF sample undergoes severe mass loss at elevated temperatures, with a residual mass of approximately 30% at 900 ℃, signifying inferior thermal stability. The thermal stability of the LSRF/20AG sample is superior to that of LSRF. However, it still exhibits a distinct mass loss process, with a residual mass of about 40% at 900 ℃. This outcome reflects the limited thermal stability enhancement achieved by a single filler. In contrast, the ternary composite filler system exhibits a marked reduction in thermogravimetric rate, with a residual mass exceeding 50% at 900 ℃. In particular, the residual mass of the LSRF/30KL10GP20AG sample reaches

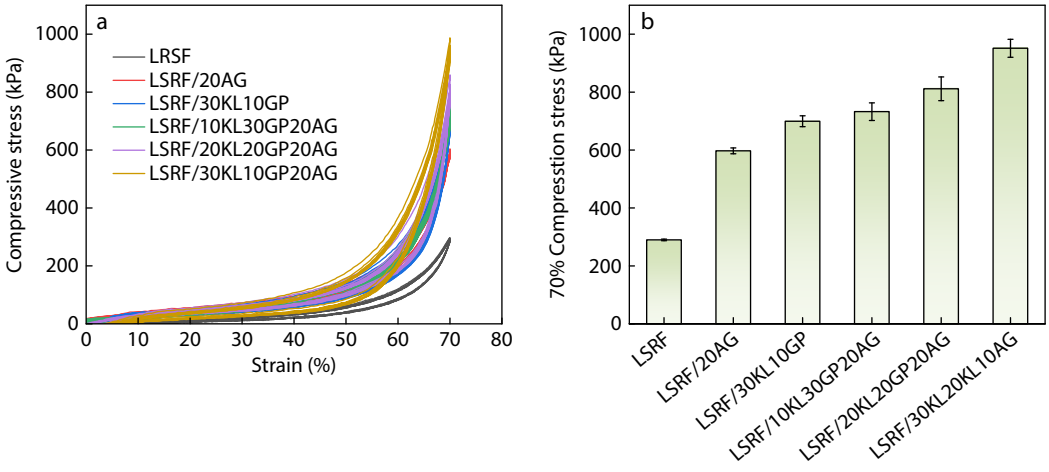

Fig. 6 Effects of different flame-retardant fillers on the material: (a) compressive performance, (b) 70% compressive strength.

https://doi.org/10.1007/s10118-026-3612-y

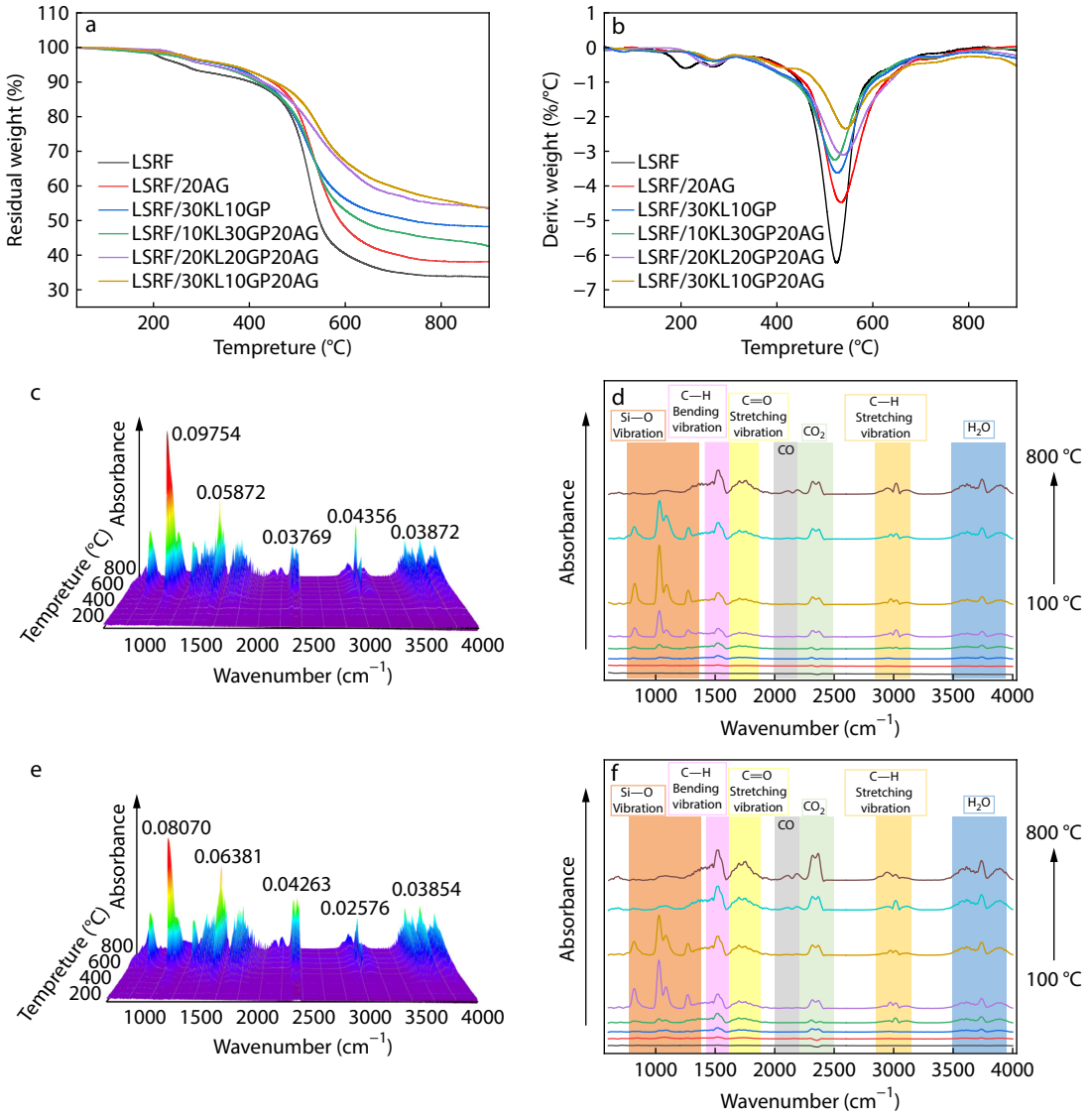

Fig. 7 Thermogravimetric curves of flame-retardant LSRF foams: (a) TG, (b) DTG; TG-IR spectra: (c, d) LSRF, (e, f) LSRF/30KL10GP20AG.

53.7%. This remarkable performance stems from the formation of a denser ceramic layer by composite fillers at high temperatures *via* a multi-component synergistic ceramification effect, which effectively hinders matrix thermal degradation and thereby significantly enhances the thermal stability of the material.[21] In Fig. 7(b), the DTG curve of LSRF exhibits a sharp mass loss peak with a high band mass loss rate, demonstrating that its thermal degradation process is concentrated and intense. In contrast, the DTG curves of the composite filler systems are broadened, and their peak mass loss rates are significantly reduced, with the LSRF/30KL10GP20AG system showing the smallest peak mass loss rate in particular. This trend indicates that the introduction of composite fillers shifts the material's thermal degradation from a rapid, concentrated process to a slow, dispersed one. The underlying mechanism is that the multi-component synergistic effect improves the thermal stability and ceramification performance of fillers, retards the matrix thermal decomposition rate, and thus optimizes the material's thermal behavior.[22] Therefore, these results confirm that the LSRF/30KL10GP20AG sample exhibits the highest thermal stability.

Subsequently, Figs. 7(c)–7(f) focus on showing the three-dimensional and two-dimensional stacked infrared spectra of the gases released during the thermal decomposition of the flame-retardant silicone rubber foam, respectively. We can clearly see from Figs. 7(c) and 7(e), compared with LSRF, the sample LSRF/30KL10GP20AG shows a significant reduction in band intensity in the ranges of 700–1200 and 2800–3100 cm^{-1}, whereas the band intensity at 2360 cm^{-1} increases. This variation is attributed to the formation of a dense ceramic layer on the material surface after the ceramification reaction, which effectively impedes the thermal decomposition of the internal silicone rubber foam. Additionally, it can also be found from Figs. 7(d) and 7(f) that LSRF still undergoes intense Si—O bond decomposition reaction at approximately 700 °C, whereas the peak of sample LSRF/30KL10GP20AG at 700 °C has already reached a stable stage. This finding verifies that the synergistic effect of fillers such as KL, GP, and AG

enhances the stability of Si—O bonds, inhibits structural collapse at high temperatures, and reduces internal thermal decomposition.[23] Notably, no large quantities of toxic gases are generated during combustion throughout the entire process, with only slight fluctuations of CO detected. This characteristic further confirms the low toxicity of the foam during combustion.

Flame Retardant Performance and Combustion Behavior of Different Flame Retardant LSRF

In this study, we systematically evaluated the vertical burning behavior, LOI, and micromorphology of the samples before and after combustion. As shown in the Fig. 8(a), the LSRF sample is extremely flammable and continues to burn after the flame is removed, showing poor flame-retardant performance. Fig. 8(b) reveals that the LSRF/30KL10GP sample is relatively easy to ignite. After the flame is removed, it exhibits a self-extinguishing tendency but still continues to burn, reflecting a certain improvement in flame-retardant performance compared to the LSRF sample. Notably, the LSRF/30KL10GP20AG sample (Fig. 8c) demonstrated significantly enhanced flame resistance, with slower flame spread, a confined burning area, and rapid self-extinguishing behavior (within ≤1 s after each ignition) without dripping. The underlying reason is that GP and KL form an expanded ceramic barrier during initial combustion, protecting the foam and isolating oxygen, while AG can inhibit heat conduction.[24] The foam is not easily ignited during the second ignition and still exhibits rapid self-extinguishing behavior after ignition. This is due to the formation of a uniform and dense ceramic layer at the bottom in contact with the flame. At this time, the self-extinguishing tendency of the foam during combustion is more obvious, reflecting the synergistic effect of flame-retardant components in gas-phase flame inhibition and condensed-phase ceramification, which effectively hinders the continuous spread of the flame. Fig. 8(d) and Table S1 (in ESI) manifests that the limiting oxygen index of LSRF composites with different formulations. The LSRF sample has an LOI of only 24.0%, is classified as flammable, and only reaches the V-1 grade in the vertical burning test. The LSRF/20AG sample has an LOI of 26.6%, demonstrating initial flame retardancy performance. The addition of KL, GP, and AG gradually improves flame-retardant efficiency, and flame-retardant performance can be further enhanced by adjusting the proportions of the different fillers. Among them, the LSRF/30KL10GP20AG sample with the best flame-retardant performance reaches the V-0 grade in the vertical burning test, with an LOI value of 33.2% simultaneously. The above results indicate that the type and compound degree of flame-retardant components play a key regulatory role in the combustion behavior and LOI of the material. The multi-component composite filler system can significantly improve the combustion grade of the material and enhance its flame-retardant performance through the synergistic effect of multiple mechanisms.[25] As can be seen from the material before combustion in Fig. 8(e), the foam interior and surface display a rough morphology with filler particles combined with the matrix, verifying effective dispersion of flame-retardant fillers in the matrix. After combustion, a dense ceramic layer structure composed of numerous accumulated particles is formed both internally and on

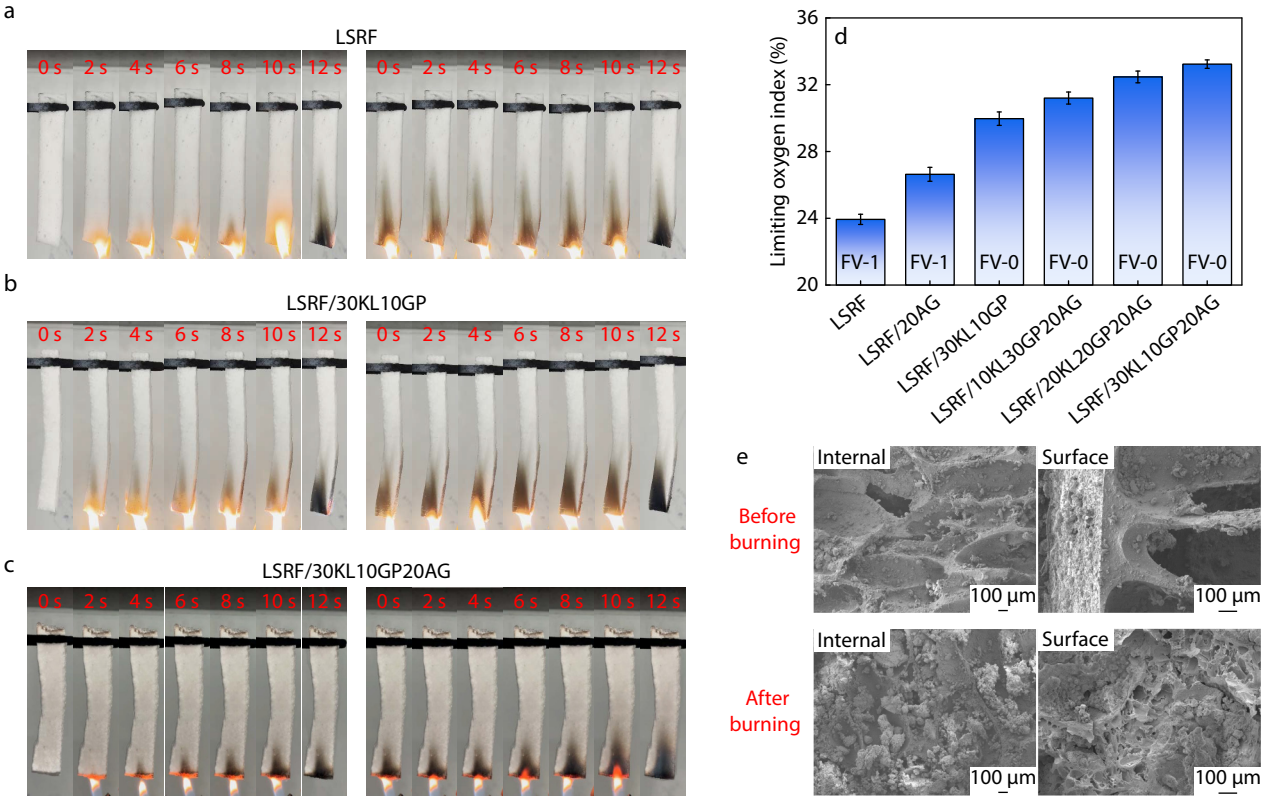

Fig. 8 Vertical burning: (a) LSRF, (b) LSRF/30KL10GP, (c) LSRF/30KL10GP20AG during the first and second ignition; (d) LOI test; (e) Internal and surface microstructure of sample LSRF/30KL10GP20AG before and after burning.

the surface. This demonstrates that flame-retardant fillers effectively impede internal flame propagation during combustion and, when synergistically ceramified, form a robust ceramic barrier that blocks heat and oxygen transfer. Furthermore, the material possesses excellent hydrophobicity with a water contact angle of 160.35° (Fig. S3 in ESI), thereby further enhancing its flame-retardant performance.[26]

Cone calorimeter test is a core method for evaluating the fire safety performance of materials, with key indicators including heat release rate (HRR), total heat release (THR), and total smoke production (TSP).[27] According to Fig. 9(a), the LSRF burns very rapidly after ignition, exhibiting an extremely sharp HRR peak with a peak HRR as high as 125 kW/m^2. However, after the incorporation of fillers, the HRR curves of the foams become gradually flattened. Among all samples, the LSRF/30KL10GP20AG sample achieves the lowest HRR of 63 kW/m^2, representing a 49.6% reduction compared with the LSRF. This indicates that the synergistic flame-retardant effect of KL, GP, AG, and LSRF slows down the combustion rate of the composite foam and effectively suppresses heat release. Based on the findings in Fig. 9(b), the THR of the LSRF rises rapidly over time, reaching nearly 39 MJ/m^2 at 400 s. By comparison, the THR growth rate of composite systems is significantly reduced, with the LSRF/30KL10GP20AG system exhibiting the lowest THR of only 25.2 MJ/m^2 at 1000 s. This further validates the synergistic advantages of multi-component fillers in blocking heat transfer and inhibiting heat release.[28] Smoke generation during combustion is a crucial factor associated with fire safety. It can be observed from Fig. 9(c) that the peak TSP of the LSRF is approximately 5.8 m^2, while the TSP of the composite systems is significantly reduced. In particular, the LSRF/30KL10GP20AG system shows a TSP as low as 0.94 m^2, indicating that the introduction of fillers can effectively inhibit smoke generation and improve personnel safety in fire scenarios. The macroscopic morphology after ceramification directly reflects the structural stability of materials under high temperatures. Fig. 9(d) provides evidence that the LSRF exhibits obvious cracking, shrinkage and collapse after ceramification, with poor structural integrity. In contrast, the ceramified products of composite systems (*e.g.*, LSRF/30KL10GP20AG) show significantly fewer surface cracks and a much denser overall structure. This suggests that the synergistic ceramification effect of multi-component fillers forms a continuous ceramic layer, which effectively maintains structural integrity at high temperatures.[29] Fig. 9(e) compares the LOI values, HRR, and density of LSRF/30AG10KL20AG with other previously reported liquid silicone foams. The ceramifiable liquid silicone foam in this study exhibited a high oxygen index of 33.2%, reduced the heat release rate to 63 kW/m^2, and maintained a very low density of 0.259 g/cm^3.[30–34]

Thermal conductivity serves as a critical parameter for assessing the thermal insulation performance of materials, where lower values correspond to superior insulation capabil-

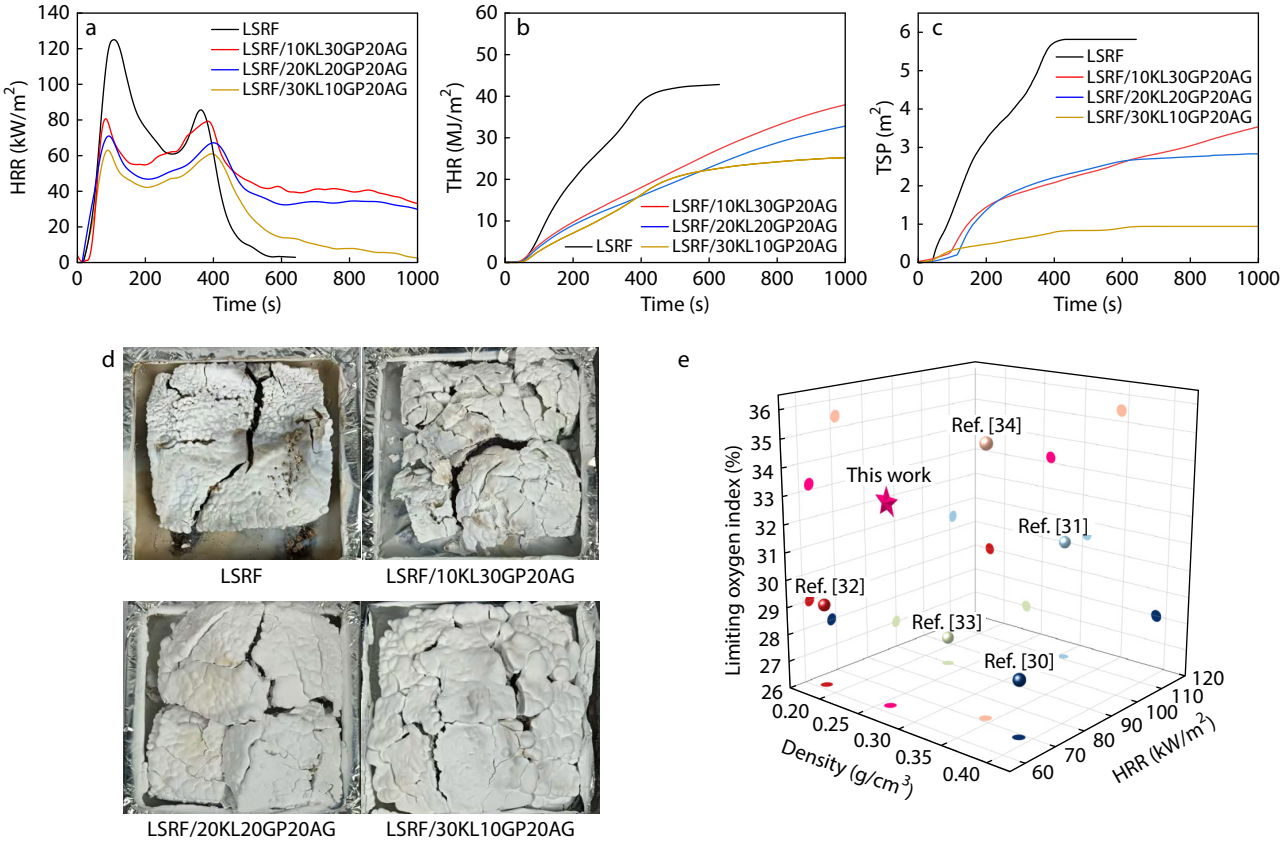

Fig. 9 Different flame-retardant LSRF: (a) HRR, (b) THR, (c) TSP; (d) Residual photographs after combustion; (e) Comparison diagram of limiting oxygen index, HRR and density from different literatures.

ity. As illustrated in Fig. 10(a), the thermal conductivities of various LSRF samples exhibit considerable variation across different formulations. The LSRF sample shows a thermal conductivity of 0.112 W/(m·K), indicating a comparatively high thermal conduction characteristic. Upon incorporation of composite fillers, most modified systems demonstrate reduced thermal conductivity, except for the 30KL10GP binary system. Notably, the 20AG sample achieves the lowest value of 0.056 W/(m·K), which can be attributed to the low density and high porosity of AG that introduce numerous thermal insulation cavities within the material. Additionally, the interfaces between AG particles effectively scatter phonons involved in heat transfer, thereby significantly suppressing thermal conductivity. In contrast, the 30KL10GP system exhibits a thermal conductivity higher than that of the sample. This increase likely results from the disruption of the original insulating microstructure of the matrix by the combined presence of KL and GP, along with enhanced thermal pathways due to filler-filler contact.[35] By comparison, all ternary filler systems display lower thermal conductivities than the LSRF and are markedly improved relative to the 30KL10GP binary system. This improvement stems from the dominant insulating contribution of AG, whose intrinsic pore-based insulation capability outweighs the structural disruption effect induced by KL and GP. Among these, the 30KL10GP20AG composite registers a thermal conductivity of 0.065 W/(m·K). Although slightly higher than that of the 20AG sample, this system holds greater practical relevance when considering its balanced overall performance in flame retardancy, mechanical properties, and other functional aspects.

Flame-retardant foam materials that exhibit high-efficiency flame impact resistance and thermal insulation can maintain structural integrity under fire exposure, thereby providing critical time for personnel evacuation and fire-fighting operations.[36,37] Referring to Figs. 10(b) and 10(c), distinct differences in flame-impact resistance and thermal insulation performance are observed among the various LSRF samples. This study systematically examined the flame-retardant proper-

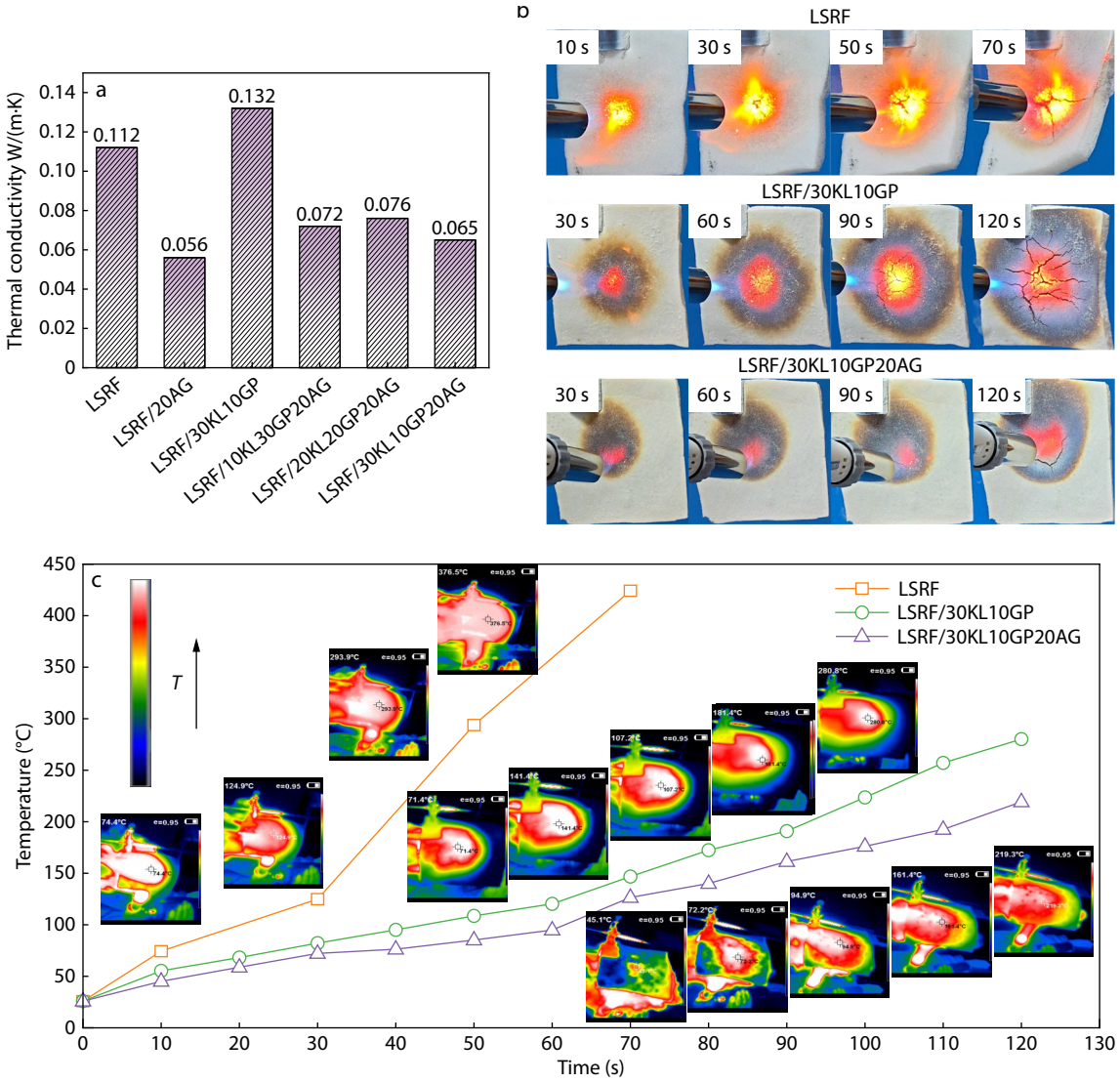

Fig. 10 Flame-retardant of LSRF. (a) Thermal insulation performance chart; (b) Digital photos of the flame impact test; (c) Variation of the back surface temperature with flame impact time.

https://doi.org/10.1007/s10118-026-3612-y

ties of LSRF, LSRF/30KL10GP, and LSRF/30KL10GP20AG from two perspectives: macroscopic combustion behavior and temperature-time dynamic response. In terms of macroscopic combustion behavior (Fig. 10b), the LSRF sample exhibited rapid flame spread, with visible open flames emerging within 10 s and a notably expanded combustion area by 70 s, indicating intense burning. The LSRF/30KL10GP sample exhibited reduced combustion severity and a lower flame propagation rate, although a relatively clear combustion zone persisted. In contrast, the LSRF/30KL10GP20AG sample demonstrated significantly suppressed combustion behavior, with no obvious open flames throughout the test and only localized thermal response. These results suggest that incorporating AG produces a synergistic flame-retardant effect with KL and GP, leading to the formation of a stable ceramic-layer structure that effectively hinders flame propagation and spread.[38] Regarding the temperature-time dynamic response (Fig. 10c), the surface temperature of the LSRF sample rose rapidly, reaching nearly 450 °C at 120 s, with a very high heating rate. The temperature rise of LSRF/30KL10GP was noticeably suppressed, attaining about 300 °C at 120 s, indicating that the combination of KL and GP can preliminarily lower the material's heat release rate. The LSRF/30KL10GP20AG sample displayed the mildest temperature response, reaching only 219 °C at 120 s with a significantly slowed heating rate. This is attributed to the multi-component synergistic system composed of AG, KL, and GP, which not only enhances the thermal insulation and oxygen-barrier effects of the ceramic layer but also leverages the excellent insulating performance of AG, thereby achieving efficient regulation of the material's thermal behavior.[39] To summarize, the composite design of fillers, through the synergistic action of multi-component flame-retardant mechanisms, can markedly improve the flame-retardant performance of materials, specifically manifested in the inhibition of flame spread, reduction of peak surface temperature, and deceleration of the heating rate. This study provides an experimental basis for the development of high-performance flame-retardant materials. It holds considerable application value and theoretical reference significance for fields with stringent flame-retardancy requirements, such as construction and electrical engineering.

Ceramifiable Behavior of LRSF Composites

The ceramification performance of flame-retardant LSRF was investigated (Fig. 11). Fig. 11(a) provides evidence that, with variation in filler type and content, there are significant differences in the macroscopic integrity and char residue morphology of the materials. LSRF has a small amount of char residue with a loose structure and large volume shrinkage, while the composite filler system (*e.g.*, LSRF/30KL10GP20AG) exhibits a complete char residue block. This indicates that the composite fillers can synergistically promote ceramification and maintain the structural stability of the ceramic layer.[40] It can be seen from Fig. 11(b) that the cross-section of the LSRF is rough, with a damaged cell structure. In contrast, the composite system containing AG, GP, and KL has a denser cross-section and intact cells. Notably, the sample LSRF/30KL10GP20AG has the densest ceramic layer

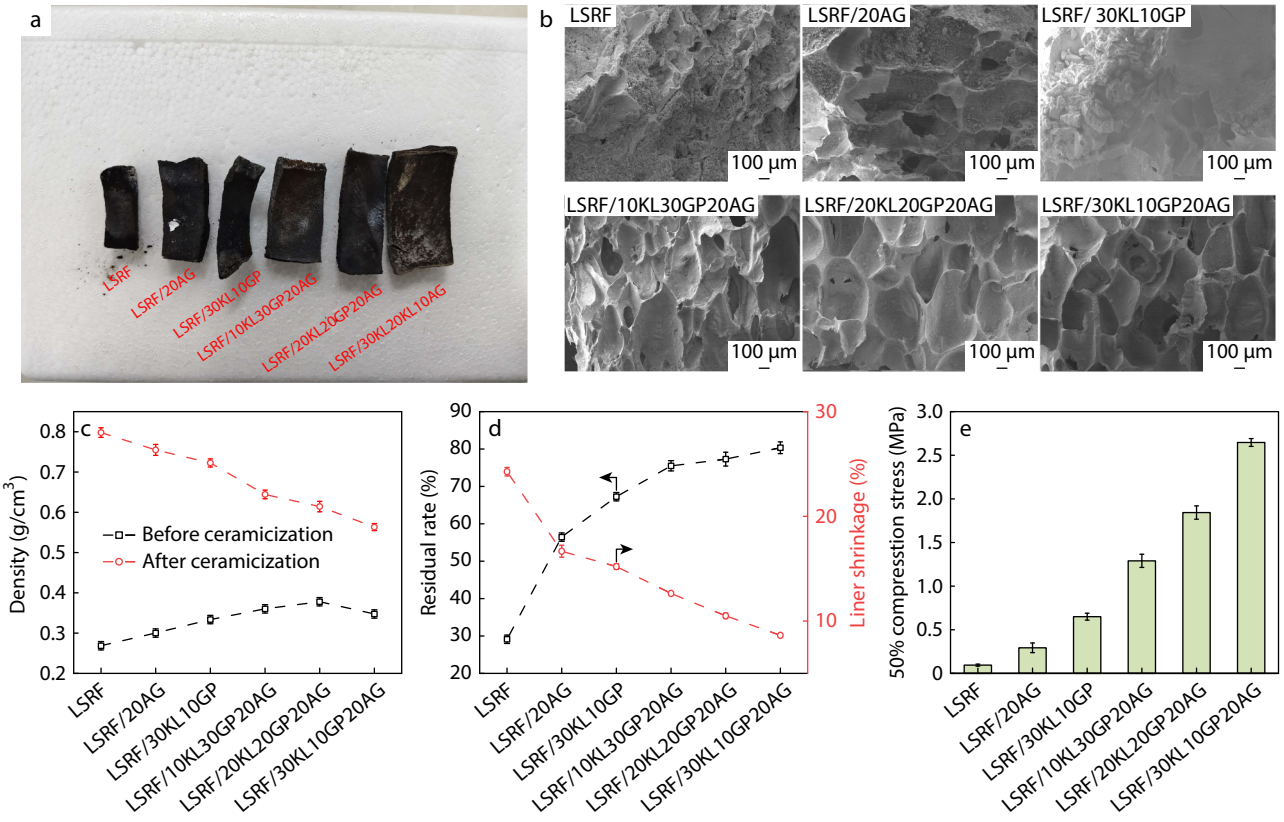

Fig. 11 Flame-retardant LSRF after ceramization: (a) sample image, (b) microstructure, (c) density before and after, (d) residual char and linear shrinkage, (e) compressive strength.

https://doi.org/10.1007/s10118-026-3612-y

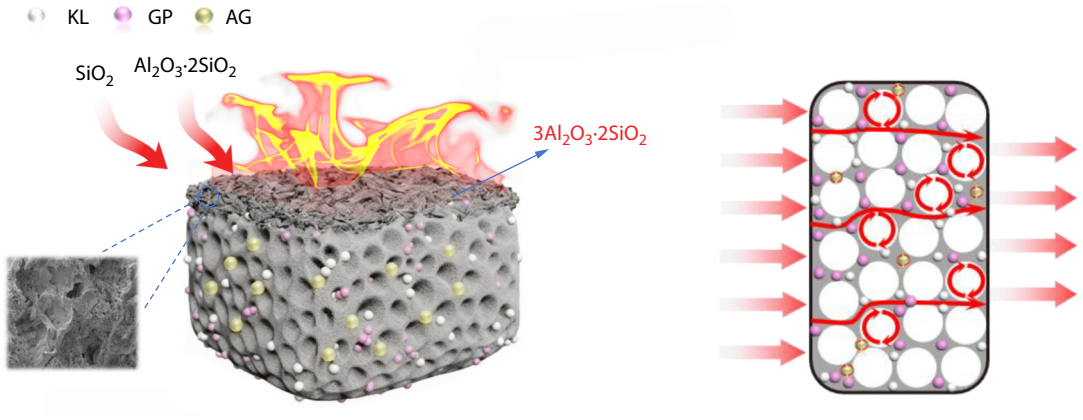

Fig. 12 Ceramization and flame retardant mechanism of flame retardant LSRF materials.

structure, suggesting that the filler particles in this formulation exhibit tight interface bonding with the matrix and a superior synergistic effect. As captured in Fig. 11(c), the density after ceramification decreases with formula optimization, reaching 0.573 g/cm^3. This is because, through optimization of the formula, the foam's volume shrinkage during ceramification is reduced, and the cell structure tends to remain stable. From the data in Fig. 11(d), it is evident that the char residue rate increases significantly with filler compounding, while the volume shrinkage rate decreases, remaining at 8.6%. This is due to the synergistic effect of gas-phase flame retardancy and condensed-phase ceramification of the composite fillers. It not only reduces the release of thermal decomposition volatiles but also blocks the transfer of heat and oxygen through the dense ceramic layer. Thereby achieving dual effects: improved char residue rate and optimized flame retardancy.[41] As detailed in Fig. 11(e), the compressive strength increases stepwise with formula optimization, and the compressive strength of sample LSRF/30KL10GP20AG is improved most significantly, reaching 2.69 MPa. The higher the KL content, the greater the foam's skeleton strength after ceramification. Coupled with the synergistic reinforcing effect of AG and GP, the ceramification performance is further enhanced. Thus, the rigid support of the fillers enhances the matrix's deformation resistance, endowing the material with greater mechanical strength.[42] The synergistic effect of the three fillers is essentially the connection and mutual enhancement of three mechanisms: catalytic ceramification, melting sealing and nano thermal insulation in time and space. This enables the foam to form a high-strength ceramic skeleton during high-temperature combustion, resulting in a tough, dense, highly thermal-insulating, and multifunctional protective layer.

Ceramization and Flame Retardant Mechanism of Flame Retardant LSRF

As shown in Fig. 12, the flame-retardant performance of the LSRF material is predominantly governed by its distinctive condensed-phase ceramification behavior and the resulting efficient flame-retardant mechanism. When the ambient temperature rises to 500–700 °C, the glass powder component within the system melts first.[43] The resulting liquid phase rapidly wets and encapsulates the SiO_2 particles and char residues generated from the pyrolysis of silicone rubber, while partially filling the macroscopic pores inside the aerogel. This process ultimately constructs a dense primary glass-silica-char ceramic composite layer. This composite layer effectively obstructs the transport pathways of oxygen and flammable gases, thereby achieving preliminary flame-retardant protection. During this stage, the acidic sites on the kaolin surface catalyze the dehydration and cross-linking reactions of the silicone rubber molecular chains, yielding substantial char residues and providing a material foundation for reinforcing the ceramic protective layer. As the temperature further exceeds 1000 °C, the role of kaolin becomes increasingly critical: it reacts with SiO_2—a pyrolysis product of silicone rubber-to form mullite crystals.[44] Although the aerogel may undergo nanostructural shrinkage, it is already encapsulated and solidified by the glass phase and the kaolin reaction products, thereby enhancing the overall stability of the ceramified structure. Furthermore, the residual nanostructure of the aerogel continues to provide additional thermal insulation. Ultimately, the material system forms a composite ceramic layer characterized by a mullite skeleton and glass-phase matrix and aerogel insulating unit. This ceramic layer exhibits high compactness, structural robustness, and excellent thermal insulation performance, thereby conferring efficient and durable flame-retardant properties to the material.

CONCLUSIONS

In summary, we demonstrate a simple and effective method to enhance the flame retardancy and ceramifiability of LSRF. First, the particle leaching method was employed to improve the open-cell performance of the silicone rubber foam, achieving a water absorption rate of 242% and a porosity of 76.2% while maintaining excellent flexibility. Subsequently, the foam was modified by vacuum-impregnating ceramifiable flame-retardant fillers. Benefiting from the efficient synergistic effect among KL, GP, and AG fillers, the flame-retardant performance of the LSRF/30KL10GP20AG sample was significantly improved-it passed the UL-104 V-0 rating with a LOI of 33.2%, HRR decreased by 49.6%. The silicone rubber foam exhibited self-extinguishing behavior without generating droplets during combustion. After combustion, the surface exhibited excellent hydrophobicity, with a water contact angle exceeding 160°. In addition, under high-temperature combustion, a high-strength ceramic layer structure was formed, accompanied by reduced foam shrinkage, well-preserved cell structure, and high cerami-

https://doi.org/10.1007/s10118-026-3612-y

fied compressive strength (nearly 3 MPa), indicating remarkably enhanced ceramification performance of the foam. Leveraging these advantages, this open-cell, flame-retardant silicone rubber foam has great potential for various practical applications and can be used to fabricate thermal insulation building materials with superior flame-retardant performance.

Conflict of Interests

The authors declare no interest conflict.

Electronic Supplementary Information

Electronic supplementary information (ESI) is available free of charge in the online version of this article at http://doi.org/10.1007/s10118-026-3612-y.

Data Availability Statement

The data that support the findings of this study are available from the corresponding author upon reasonable request.

ACKNOWLEDGMENTS

This work was financially supported by the Natural Science Foundation of Qingdao Municipality (No. 25-1-1-99-zyyd-jch) and the Natural Science Foundation of Shandong Province (No. ZR2024QE446).

REFERENCES

1 Hu, F.; Wu, S.; Sun, Y. Hollow-structured materials for thermal insulation. *Adv. Mater.* **2019**, *31*, 1801001.
2 Han, T. L.; Guo, B. F.; Zhang, G. D.; Tang, L. C. Facile synthesis of hollow glass microsphere filled PDMS foam composites with exceptional lightweight, mechanical flexibility, and thermal insulating property. *Molecules* **2023**, *28*, 2614.
3 Lou, F.; Yan, W.; Guo, W.; Li, Q. Preparation and properties of ceramifiable flame-retarded silicone rubber composites. *J. Therm. Anal.* **2017**, *130*, 813–821.
4 Song, J.; Zhang, X.; Wang, J.; Sun, J.; Shi, A. Ceramifiable flame-retarded silicone rubber composites based on novel phosphorus/nitrogen/silicon-containing flame retardants. *Silicon* **2023**, *15*, 5001–5011.
5 Wang, X.; Huang, A.; Zhao, M.; Li, J.; Li, S.; Li, X. Preparation and ablation properties study of a single component ceramifiable RTV silicone rubber. *J. Rubber Res.* **2023**, *26*, 391–405.
6 Li, P.; Jin, H.; Wei, S.; Liu, H.; Gao, N.; Shi, Z. Ceramization mechanism of ceramizable silicone rubber composites with nano silica at low temperature. *Materials* **2020**, *13*, 3708.
7 Wang, Q. Z.; Cui, C. X.; Liu, S. J.; Zhao, L. C. Open-celled porous Cu prepared by replication of NaCl space-holders. *Mater. Sci. Eng. A* **2010**, *527*, 1275–1278.
8 Shang, K.; Lin, G. D.; Jiang, H. J.; Jin, X.; Zhao, J.; Liu, D.; Zhao, B.; Yang, J. J.; Fu, T.; Wang, J. S. Flame retardancy, combustion, and ceramization behavior of ceramifiable flame-retardant room temperature vulcanized silicone rubber foam. *Fire Mater.* **2023**, *47*, 1082–1091.
9 Lin, T.; Shang, K.; Lin, G. D.; Wang, J. S.; Yang, J. J. Ceramifiable flame-retardant silicone rubber foam for long-term fire resistance and thermal insulating. *Chem. Eng. J.* **2025**, *519*, 165733.
10 Liu, X.; Ma, L.; Sheng, Y.; Liu, S.; Wei, G.; Wang, X. Synergistic flame-retardant effect of modified hydrotalcite and expandable graphite for silicone rubber foam. *J. Appl. Polym. Sci.* **2023**, *140*, e53471.
11 Han, Y.; Yang, L.; Yu, Z.; Zhao, Y.; Zhang, Z. X. Lightweight and flame retardant silicone rubber foam prepared by supercritical nitrogen: The influence of flame retardants combined with ceramicizable fillers. *Constr. Build. Mater.* **2023**, *370*, 130735.
12 Wang, Z.; Wang, C.; Gao, Y.; Li, Z.; Shang, Y.; Li, H. Porous thermal insulation polyurethane foam materials. *Polymers* **2023**, *15*, 3818.
13 Zhang, Y.; Jing, M.; Zhang, M.; Hou, S.; Zhang, B. Preparation and properties of silica gel foam as fire-retardant with high water retention for wood. *Fire Technol.* **2022**, *58*, 3597–3621.
14 Peng, L.; Lei, L.; Liu, Y.; Du, L. Improved mechanical and sound absorption properties of open cell silicone rubber foam with NaCl as the pore-forming agent. *Materials* **2021**, *14*, 195.
15 Li, Y.; Wang, Z.; Guo Z. Preparation and compression behavior of high porosity, microporous open-cell Al foam using supergravity infiltration method. *Materials*, **2024**, *17*, 36.
16 Omidi-Ghallemohamadi, M.; Ahmadi-Khaneghah, A.; Behniafar, H. Epoxy networks possessing polyoxyethylene unites and loaded by Jeffamine-modified graphene oxide nanoplatelets. *Prog. Org. Coat.* **2019**, *134*, 264–271.
17 Park, J. H.; Minn, K. S.; Lee, H. R.; Yang, S. H.; Yu, C. B.; Pak, S. Y.; Oh, C. S.; Song, Y. S.; Kang, Y. J.; Youn, J. R. Cell openness manipulation of low density polyurethane foam for efficient sound absorption. *J. Sound Vib.* **2017**, *406*, 224–236.
18 Aghaei, P.; Visconti, C. G.; Groppi, G.; Tronconi, E. Development of a heat transport model for open-cell metal foams with high cell densities. *Chem. Eng. J.* **2017**, *321*, 432–446.
19 Chen, J.; Li, X.; Li, W.; He, J.; Li, C.; Dai, S.; Chen, J.; Ren, Y. Study on the compression properties and deformation failure mechanism of open-cell copper foam. *Adv. Eng. Mater.* **2017**, *19*, 1600861.
20 Karimi, E. Z.; Barzegar, F.; Moloodi, A.; Zolfaghari, R. Hardness and compressive properties of open-cell nickel foam reinforced by nano-SiC particles. *Metall. Mater. Trans. B* **2021**, *52*, 3439–3446.
21 Fu, H.; Yin, D.; Wang, T.; Gong, W.; Zhou, H. Open pore morphology evolution in poly(butylene succinate)/chitin nanocrystal nanocomposite foams. *J. Polym. Environ.* **2022**, *30*, 401–414.
22 Durif, C.; Wynn, M.; Balestrat, M.; Kim, Y. W.; Leriche, A.; Miele, P.; Colombo, P. Open-celled silicon carbide foams with high porosity from boron-modified polycarbosilanes. *J. Eur. Ceram. Soc.* **2019**, *39*, 5114–5122.
23 Parker, S. F.; Klehm, U.; Albers, P. W. Differences in the morphology and vibrational dynamics of crystalline, glassy and amorphous silica-commercial implications. *Mater. Adv.* **2020**, *1*, 749–759.
24 Zhuo, H.; Chen, Y.; Xie, H.; Huang, X.; Guro, V. P.; Tadjiev, K.; Li, Y. Nanoporous silica-chitosan aerogels for thermal insulation and flame retardancy. *ACS Appl. Nano Mater.* **2024**, *7*, 4784–4795.
25 Li, M.; Bi, S.; Chen, C.; Hai, W.; Jiang, Z.; Meng, Q.; Hao, E.; Li, H.; Shao, H., Shao, G.; Jiang, J.; Chen, N. Comparison of multi-component and mono-component intumescent flame retardants for thermoplastic polyurethane composites. *J. Vinyl Addit. Technol.* **2024**, *30*, 997–1009.
26 Cao, J.; Wang, D.; Wang, L.; Feng, S. A Superhydrophobic and oleophobic silicone sponge with hierarchical structures. *Macromol. Rapid Commun.* **2021**, *42*, 2000761.
27 Yu, S.; Liu, Y.; Cao, J.; Wen, S.; Zhang, Z. Supercritical N_2-induced lightweight high-strength chloroprene rubber foam with excellent flame-retardant and smoke suppression. *Composites, Part A.* **2025**, *190*, 108663.

Graphical Abstract

Ceramizable Perforated Silicone Foam for Thermal Insulation and Refractory Building Materials

Xiang-Yuan Tian, Xin Zhang, Dian-Bo Zhang, Ya Liu, Xiao-Pei Wang, and Zhen-Xiu Zhang

Qingdao University of Science and Technology

The diagram presents two scenarios: the material undergoes ceramization at high temperatures to achieve flame retardancy and heat insulation, while retaining heat at low temperatures to reduce heat loss, demonstrating its excellent flame-retardant, heat-insulating, and thermal preservation properties.

Chinese J. Polym. Sci., 2026 *https://doi.org/10.1007/s10118-026-3612-y*

28 Yu, Z.; Song, Y.; Yang, L.; Wen, S.; Zhao, Y.; Zhang, Z. Lightweight and flame retardant fluorosilicone rubber composited foam prepared by supercritical nitrogen. *J. Vinyl Addit. Technol.* **2023**, *29*, 901–908.

29 Jiang, Z.; Chen, Z.; An, Y.; Wang, S.; Li, T.; Liu, H.; Zhang, H.; Yang, W.; Lu, H.; Wei, C. Fire retardancy properties of ceramifiable polydimethylsiloxane/hydroxyapatite composites. *J. Appl. Polym. Sci.* **2025**, *142*, e57597.

30 Wu, Z.; Zhao, Y.; Li, H.; Zeng, X.; Lin, J.; Wu, J.; Zhou, Y.; Chen, G.; Lai, X. Multifunctional ceramifiable silicone foam for smart fire fighting. *Chem. Eng. J.* **2024**, *496*, 154149.

31 Wang, S.; Chen, Y.; Zhang, J.; Wang, T.; Niu, Y.; Wang, J. Enhanced flame retardancy of polyurethane foam with alginate-based flame-retardant coating. *Int. J. Biol. Macromol.* **2025**, *289*, 138968.

32 Wu, Q.; Zhang, Q.; Zhao, L.; Li, S. N.; Wu, L. B.; Jiang, J .X.; Tang, L. C. A novel and facile strategy for highly flame retardant polymer foam composite materials: transforming silicone resin coating into silica self-extinguishing layer. *J. Hazard. Mater.* **2017**, *336*, 222–231.

33 Cao, C. F.; Wang, P. H.; Zhang, J. W.; Guo, K. Y.; Li, Y.; Xia, Q. Q.; Zhang ,G. D.; Zhao, L.; Chen, H.; Wang, L. One-step and green synthesis of lightweight, mechanically flexible and flame-retardant polydimethylsiloxane foam nanocomposites via surface-assembling ultralow content of graphene derivative. *Chem. Eng. J.* **2020**, *393*, 124724.

34 Shang, K.; Jiang, H.; Zhao, J.; Zhao, B.; Jin, X.; Lin, G.; Yang, J.; Wang, J. Fabrication of CoFe-layered double hydroxide for flame retardant and smoke suppression of silicone rubber foam. *J. Appl. Polym. Sci.* **2024**, *141*, e56087.

35 Hur, K.; Lee, H. J.; Wi, S.; Chang, S. J.; Kim, S. Barrier effect of insulation against harmful chemical substances according to the wall surface construction of layered building materials. *Constr. Build. Mater.* **2023**, *368*, 130430.

36 Hoehn, R. M.; Jahl, L. G.; Herkert, N. J.; Hoffman, K.; Soehl, A.; Diamond, M. L.; Blum, A.; Stapleton, H. M. Flame retardant exposure in vehicles is influenced by use in seat foam and

temperature. *Environ. Sci. Technol.* **2024**, *58*, 8825−8834.
37 Cao, C. F.; Yu, B.; Guo, B. F.; Hu, W. J.; Sun, F. N.; Zhang, Z. H.; Li, S. N.; Wu, W.; Tang, L. C.; Song, P.; Wang, H. Bio-inspired, sustainable and mechanically robust graphene oxide-based hybrid networks for efficient fire protection and warning. *Chem. Eng. J.* **2022**, *439*, 134516.
38 Dong, F.; Wang, Y.; Wang, S.; Shaghaleh, H.; Sun, P. Flame-retarded polyurethane foam conferred by a bio-based nitrogen-phosphorus-containing flame retardant. *React. Funct. Polym.* **2021**, *168*, 105057.
39 Xi, W.; Qian, L.; Li, L. Flame retardant behavior of ternary synergistic systems in rigid polyurethane foams. *Polymer* **2019**, *11*, 207.
40 Zhao, D.; Kong, L.; Wang, J.; Jiang, G.; Zhang, J.; Shen, Y.; Wang, T. Ceramifiable silicone rubber composites with enhanced self-supporting and ceramifiable properties. *Polymer* **2022**, *14*, 1944.
41 Zhao, D.; Liu, T.; Xu, Y.; Zhang, J.; Shen, Y.; Wang, T. Investigation of the thermal degradation kinetics of ceramifiable silicone rubber-based composite. *J. Therm. Anal.* **2023**, *148*, 6487−6499.
42 Li, S.; Wei, C.; Zhou, L.; Wang, P.; Wang, W. Microstructure and fracture strength of silicon nitride ceramics consolidated by oscillatory pressure sintering. *Ceram. Int.* **2019**, *45*, 15671−15675.
43 Zhao, Z.; Li, C.; Yu, R.; Le, L.; Liu, M,; Zhang, Z. A lava-inspired ceramicized strategy to fabricate flame retardant coating with glass powder and boron nitride for wood fire prevention. *Appl. Surf. Sci*. **2025**, 164551.
44 Hou, Z.; Liu, C.; Liu, L.; Zhang, S. Microstructural evolution and densification behavior of porous kaolin-based mullite ceramic added with MoO_3. *Ceram. Int.* **2018**, *44*, 17914−17918.

https://doi.org/10.1007/s10118-026-3612-y